http://dx.doi.org/10.5012/bkcs.2013.34.6.1814

Theoretical Study on Interactions between *N*-Butylpyridinium Nitrate and Thiophenic Compounds

Renqing Lü,[*] Dong Liu,[†] Shutao Wang, and Yukun Lu

College of Science, China University of Petroleum (East China), Qingdao, 266580, Shandong Province, China
[*]*E-mail: lvrq2000@163.com*
[†]*College of Chemical Engineering, China University of Petroleum (East China), Qingdao, 266580, Shandong Province, China*
Received January 14, 2013, Accepted March 24, 2013

By using density functional theory calculations, we have performed a systemic study on the electronic structures and topological properties of interactions between *N*-butylpyridinium nitrate ($[BPY]^+[NO_3]^-$) and thiophene (TS), benzothiophene (BT), dibenzothiophene (DBT), naphthalene (NAP). The most stable structure of $[BPY]^+[NO_3]^-$ ion pair indicates that hydrogen bonding interactions between oxygen atoms on $[NO_3]^-$ anion and C2-H2 on pyridinium ring play a dominating role in the formation of ion pair. The occurrence of hydrogen bonding, π···H-C, and π···π interactions between $[BPY]^+[NO_3]^-$ and TS, BT, DBT, NAP has been corroborated at the molecular level. But hydrogen bonding and π···π interactions between $[BPY]^+[NO_3]^-$ and NAP are weak in terms of structural properties and NBO, AIM analyses. DBT is prior to adsorption on *N*-butylpyridinium nitrate ionic liquid.

Key Words : Ionic liquid, Density functional theory, Thiophene, Benzothiophene, Dibenzothiophene

Introduction

The desulfurization of fuel has received worldwide attention because environmental regulation of the sulfur limit for fuels is becoming increasingly stringent. Conventional hydrodesulfurization (HDS) is more effective for removal of aliphatic sulfur compounds than removal of sulfur containing aromatic compounds, such as thiophene, benzothiophene, and dibenzothiophene series. HDS requires high temperature and high hydrogen pressure in order to eliminate the alicyclic sulfur compounds.[1] Alternative sulfur removal techniques should be explored. In the past years, ionic liquids have gained increasing interest due to its unique properties both as extractant and catalyst.[2] Ionic liquids have been classified as ionic compounds that have melting points at temperatures of 100 °C or lower. The first attempt of deep desulfurization using ionic liquids was made by Wasserscheid and Jess in 2001.[3] The use of ionic liquids as media for liquid–liquid extractions is growing rapidly, since their hydrophobic or hydrophilic nature can be modulated by modifications in both cation and anion. Lo *et al.* firstly investigated removing sulfur-containing compounds from light oils by a combination of both chemical oxidation and solvent extraction using room temperature ionic liquids, 1-butyl-3-methylimidazolium hexafluorophosphate and 1-butyl-3-methylimidazolium tetrafluoroborate.[4] Following their reports, sulfur and nitrogen removals by extraction or oxidative desulfurization using ionic liquids have been reported by many research groups.

Large numbers of investigations on these subjects were performed by means of simulations. The quantum chemical based COnductor-like Screening MOdel for Real Solvent (COSMO-RS) was used to predict the non-ideal liquid phase activity coefficient for mixtures containing 1-ethyl-3-methyl imidazolium thiocyanate [EMIM][SCN], thiophene, quinoline, pyridine, indoline, pyrrole, and water.[5] The use of mixed ionic liquids as possible alternatives for the removal of aromatics has been studied via COSMO (COnductor like Screening MOdel).[6] Kumar and Banerjee used the COSMO-RS predictions to evaluate the performance of 264 possible cation–anion pairs in the removal of thiophene from diesel oil.[7] The simultaneous separation of thiophene and pyridine from isooctane were investigated by the non-random two liquid (NRTL) and UNIversal QUAasi-Chemical (UNIQUAC) models with 1-ethyl-3-methylimidazolium acetate [EMIM][OAc], 1-ethyl-3-methylimidazolium ethylsulfate [EMIM][$EtSO_4$], and 1-ethyl-3-methylimidazolium methylsulfonate [EMIM] [$MeSO_3$] as green solvents.[8] Aznar *et al.* used the UNIQUAC model to correlate the liquid–liquid equilibrium (LLE) of fifty ternary systems involving twelve different ionic liquids with the activity coefficient.[9] Molecular dynamics simulations of solutions of benzene in dimethylimidazolium chloride and dimethylimidazolium hexafluorophosphate have been performed to explain the better solubility of aromatic compounds compared to aliphatic compounds in the ionic liquids of dimethylimidazolium.[10] Extraction of thiophene or pyridine from *n*-heptane using ionic liquids was modeled by both NRTL and UNIQUAC approaches to correlate with the experimental results.[11] Quantum chemical calculations including natural bond orbital (NBO) analyses have also been carried out to investigate the simultaneous interactions of thiophene and pyridine with different ionic liquids, including 1-butyl-1-methyl pyrrolidinium tetrafluoroborate ([Pyr14][BF_4]), 1-butyl-1-methyl pyrrolidinium hexafluoro-phosphate ([Pry14][PF_6]), 1-butyl-4-methyl pyridinium tetrafluoroborate ([BPY][BF_4]), 1-butyl-4-methylpyridinium hexafluorophosphate ([BPY][PF_6]) and 1-benzyl-3-methylimidazolium

tetrafluoroborate ([BeMIM][BF_4]).[12] Zhang *et al.* employed multinuclear NMR spectroscopy and ab initio calculations to study the interactions between thiophene and the ionic liquids of 1-butyl-3-methylimidazolium hexafluorophosphate ($[BMIM]^+[PF_6]^-$) and 1-butyl-3-methylimidazolium tetrafluoroborate ($[BMIM]^+[BF_4]^-$).[13,14] The interaction between ethanethiol molecule and either anhydrous Fe^{III} chloride anions or 1-butyl-3-methylimidazolium ($[BMIM]^+$) cations of ionic liquids was investigated using density functional theory approach, ionic liquids containing anionic Fe^{III} species suggested excellent performance to remove sulfur compounds from natural gasoline.[15] Molecular dynamic simulations were performed to screen suitable ionic liquid for desulfurization. DBT and DBTO2 were used as model compounds to study the mechanism of desulphurization.[16] The structures, acidities and interactions between the cation and the anion of a series of task-specific acidic ionic liquids have been investigated by density functional theory method.[17] The interactions between *N,N*-dialkylimidazolium dialkylphosphate ionic liquids and aromatic sulfur compound, benzene were investigated by density functional theory.[18] The theoretical studies on desulfurization by imidazolium-based ionic liquids were highlighted. But the theoretical study on removal of sulfur by extraction of pyridinium-based ionic liquids was less reported.

Recently, pyridinium-based ionic liquids were employed to remove sulfur compounds from fuel.[19-23] The extraction mechanism of π···π interactions was proposed to interpret the higher selectivity for thiophenic compounds by pyridinium-based ionic liquids. In 2007, Wang *et al.* investigated the use of *N*-butylpyridinium nitrate ($[BPY]^+[NO_3]^-$) as solvent for deep desulfurization of fuels.[19] However, the detailed structures and conformations of interactions between $[BPY]^+[NO_3]^-$ and thiophene (TS), benzothiophene (BT), dibenzothiophene (DBT), naphthalene (NAP) are still unknown. Therefore, this work reports on an analysis of structures of $[BPY]^+[NO_3]^-$, $[BPY]^+[NO_3]^-$-TS, $[BPY]^+[NO_3]^-$-BT, $[BPY]^+[NO_3]^-$-DBT, and $[BPY]^+[NO_3]^-$-NAP complexes using quantum chemical calculations. The theoretical results here will confirm hydrogen bonding and π···π interactions between $[BPY]^+[NO_3]^-$ and TS, BT, DBT, NAP at the molecular level.

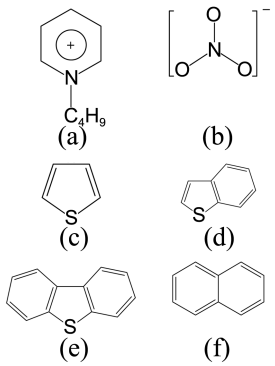

Figure 1. The structures of (a) *N*-butylpyridinium ($[BPY]^+$) (b) $[NO_3]^-$ (c) thiophene (TS) (d) benzothiophene (BT) (e) dibenzothiophene (DBT) and (f) naphthalene (NAP).

Specification of Initial Structures. The structures of *N*-butylpyridinium cation ($[BPY]^+$), $[NO_3]^-$, thiophene (TS), benzothiophene (BT), dibenzothiophene (DBT) and naphthalene (NAP) are shown in Figure 1. The $[NO_3]^-$ anion or/and TS, BT, DBT, NAP have been gradually placed in different regions around $[BPY]^+$ cation to form $[BPY]^+[NO_3]^-$, $[BPY]^+[NO_3]^-$-TS, $[BPY]^+[NO_3]^-$-BT, $[BPY]^+[NO_3]^-$-DBT, and $[BPY]^+[NO_3]^-$-NAP for optimization. The most stable structures were further employed for NBO and AIM analyses.

Computational Details. All geometric optimizations reported here were performed with DMol^3 program package.[24,25] The double numerical basis sets plus polarization functional (DNP) was employed. For the exchange correlation term of the energy functional, the generalized gradient corrected functional GGA and PW91 functional[26] as implemented in the DMol^3 program, were used for all the geometry optimizations, which are the most widely used tools for studying the geometric and electronic structures of molecules and have been shown to produce more reliable geometries for hydrogen bonding systems. Although PW91 functional is unable to provide a good description of dispersion interactions, GGA/PW91/DNP can give good results of interactions between conjugated systems.[27] All the stationary structures have been fully optimized without geometrical constraints. A frequency analysis was performed on all structures to insure the absence of imaginary frequencies. To examine the nature of interactions, the electronic properties for stationary points are illustrated based on natural bond orbital (NBO) analysis.[28] These non-local donor–acceptor-orbital interactions are associated with the delocalization of electron density between states *i* and *j* in the NBO basis, as given by

$$E(2) = \Delta E_{ij} = n_i \frac{(F_{ij})^2}{\varepsilon_j - \varepsilon_i}$$

where n_i is the donor orbital occupancy, ε_i and ε_j are the diagonal elements, and $F_{i,j}$ is the off-diagonal NBO Fork matrix element. Intermolecular interactions such as lone pair → *anti*-bonding orbital mixtures are representative of donor–acceptor bonding, whereas non-Lewis-type (highly delocalized) interactions such as anti-bond → *anti*-bond orbital mixtures represent effects like resonance stabilization.[29,30] The AIM analysis was used to analyze the nature of interactions at the B3LYP/6-31++G** level by AIM2000 package[31,32] with the wave functions generated from B3LYP/6-31++G** results.

DMol^3 uses numerical functions that are far more complete than traditional Gaussian functions, and therefore we expect BSSE contribution to be small.[33] The interaction energies between $[BPY]^+[NO_3]^-$ and TS, BT, DBT, NAP were calculated as the following expression:

$$\Delta E = -\{E([BPY]^+[NO_3]^-\text{-TS/BT/DBT/NAP}) - [E([BPY]^+[NO_3]^-) + E(\text{TS/BT/DBT/NAP})]\}$$

where $E([BPY]^+[NO_3]^-$-TS/BT/DBT/NAP) represents the energies of $[BPY]^+[NO_3]^-$-TS, $[BPY]^+[NO_3]^-$-BT, $[BPY]^+$

$[NO_3]^-$-DBT and $[BPY]^+[NO_3]^-$-NAP, $E([BPY]^+[NO_3]^-)$ and $E([BPY]^+[NO_3]^-)$, E(TS/BT/DBT/NAP) the individual energies of $[BPY]^+[NO_3]^-$, TS, BT, DBT, NAP, ΔE is the interaction energies between $[BPY]^+[NO_3]^-$ and TS, BT, DBT, NAP.

Results and Discussion

Geometries of $[BPY]^+[NO_3]^-$, $[BPY]^+[NO_3]^-$-TS, $[BPY]^+[NO_3]^-$-BT, $[BPY]^+[NO_3]^-$-DBT and $[BPY]^+[NO_3]^-$-NAP.

In this section, we discuss the most stable geometries of $[BPY]^+[NO_3]^-$, $[BPY]^+[NO_3]^-$-TS, $[BPY]^+[NO_3]^-$-BT, $[BPY]^+[NO_3]^-$-DBT and $[BPY]^+[NO_3]^-$-NAP. In order to give a visual understanding of $[BPY]^+$-NO_3^- pair interactions before the design of initial geometries for the ion-pair, the electrostatic potential surfaces for the most stable geometries of the isolated $[BPY]^+$ cation and $[NO_3]^-$ anion were constructed to gain the possible interaction modes between cation and anion shown in Figure 2, respectively. The highly negative regions of $[NO_3]^-$ anion are on the electronegative O atoms. While the highly positive regions in the $[BPY]^+$ cation are around the pyridinium ring hydrogen atoms and butyl hydrogen atoms. The possible hydrogen bonding sites on the more positively charged regions of $[BPY]^+$ cation and the more negatively charged regions of $[NO_3]^-$ anion have been taken into consideration for the initial geometry design. Correspondingly, a series of possible initial geometries for the ion-pairs were designed. The most stable structure of $[BPY]^+[NO_3]^-$ is shown in Figure 3(a). It can be seen that the

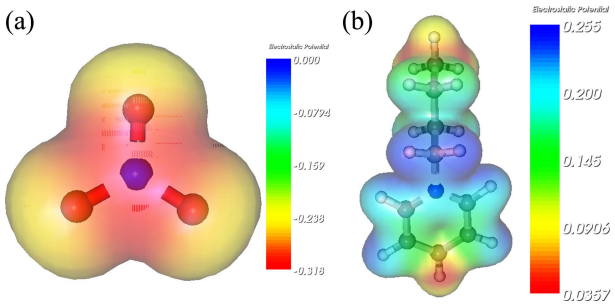

Figure 2. The electrostatic potentials (ESP) of (a) $[NO_3]^-$ anion and (b) $[BPY]^+$ cation.

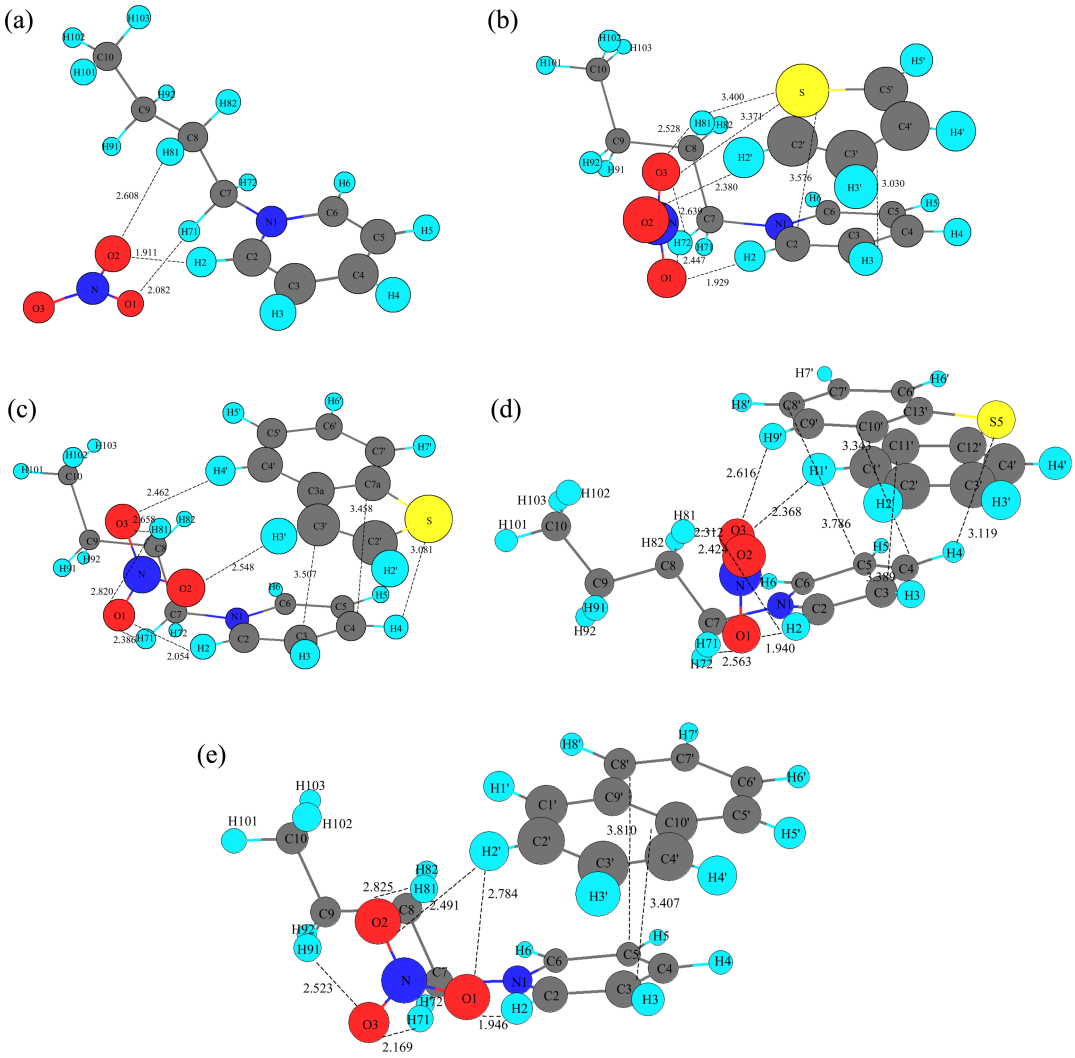

Figure 3. The optimized structures and some interacting distances (Å) of (a) $[BPY]^+[NO_3]^-$, (b) $[BPY]^+[NO_3]^-$-TS, (c) $[BPY]^+[NO_3]^-$-BT, (d) $[BPY]^+[NO_3]^-$-DBT and (e) $[BPY]^+[NO_3]^-$-NAP.

$[BPY]^+[NO_3]^-$ has three O···H interactions. The interacting distances are 1.911 Å (O2···H2), 2.082 Å (O1···H71), and 2.608 Å (O2···H81), shorter than the sum of Bondi's van der Waals radii of oxygen atom and hydrogen atom (1.52 Å and 1.20 Å).[34] The short distances of O2···H2 and O1···H71 may be ascribed to the highly positive H2 and H71 due to the withdrawing electron of nitrogen atom.

The most stable structures of $[BPY]^+[NO_3]^-$-TS, $[BPY]^+[NO_3]^-$-BT, $[BPY]^+[NO_3]^-$-DBT and $[BPY]^+[NO_3]^-$-NAP are shown in Figure 3(b)-3(e). The similar results of the strongest hydrogen bonds between one oxygen atom on $[NO_3]^-$ anion and C2-H2 on pyridinium ring are obtained for the above four structures. In the most stable $[BPY]^+[NO_3]^-$-TS, $[BPY]^+[NO_3]^-$-BT, $[BPY]^+[NO_3]^-$-DBT and $[BPY]^+[NO_3]^-$-NAP structures, the ring planes of four small molecules and pyridinium ring are parallel to each other, implying that the π-π interactions may occur. The π-π interaction (also called π-π stacking) refers to attractive non-covalent interactions between aromatic rings. Despite their frequent occurrence, there is no unifying picture of the factors that contribute to the interaction, which include electrostatic (quadrapole-quadrapole, quadrapole-dipole, and dipole-dipole), hydrophobic, and van der Waals interactions. This is complicated by the fact that aromatic rings interact in several different conformations, each of which is favored by a different combination of forces. The face-face stacked, edge-face stacked, and offset stacked geometries are three representative configurations of π-π interactions.[35,36] As shown in Figure 3(b)-3(e), the offset parallel stacking interactions between pyridinium ring and TS/BT/DBT/NAP rings occur. The offset stacked interactions are dependent on the orientation of the rings and it seems that the interactions of S···H81 (3.400 Å), S···O3 (3.371 Å), O2···H2' (2.380 Å) in $[BPY]^+[NO_3]^-$, O3···H4' (2.462 Å), O2···H3' (2.548 Å), S···H4 (3.081 Å) in $[BPY]^+[NO_3]^-$-BT, O3···H9' (2.616 Å), O3···H1' (2.368 Å), S5···H4 (3.119 Å) in $[BPY]^+[NO_3]^-$-DBT, O2···H2' (2.491 Å), O1···H2' (2.784 Å) in $[BPY]^+[NO_3]^-$-NAP may pronouncedly influence the formation of π-π interactions.[37] The interactions of S···C2 (3.576 Å), C3'···H3 (3.030 Å) in $[BPY]^+[NO_3]^-$-TS, C3'···C3 (3.507 Å), C7a···C4 (3.458 Å) in $[BPY]^+[NO_3]^-$-BT, C8'···C5 (3.786 Å), C10'···C4 (3.343 Å), C11'···C3 (3.389 Å) in $[BPY]^+[NO_3]^-$-DBT, C8'···C5 (3.810 Å), C10'···C3 (3.407 Å) in $[BPY]^+[NO_3]^-$-NAP demonstrate the occurrence of π-π interactions.

The interactions between $[BPY]^+[NO_3]^-$ and TS, BT, DBT, NAP are dependent not only on hydrogen bonds but also on π-π interactions. The sulfur atoms of TS, BT, and DBT are also involved in the interactions between TS/BT/DBT and $[BPY]^+[NO_3]^-$. The optimized structures changed with or without DFT-D method. But the optimized structures do not change significantly.

Interaction Energies. The interaction energies between $[BPY]^+[NO_3]^-$ and TS, BT, DBT, NAP are important factors in their reasonable explanations for extraction of TS, BT, DBT, and NAP by $[BPY]^+[NO_3]^-$ ionic liquids. In this work, we investigated the interaction energies between $[BPY]^+[NO_3]^-$ and TS, BT, DBT, NAP. Interaction energy (ΔE) is defined as the difference between the energy of the appointed complexes and the sum of the energies of its free fragments (components). The interaction energies between $[BPY]^+[NO_3]^-$ and TS, BT, DBT, NAP are 9.76 kcal/mol, 11.25 kcal/mol, 14.58 kcal/mol, and 7.69 kcal/mol, demonstrating that the magnitude of the interacting energies follows the trend $[BPY]^+[NO_3]^-$-NAP < $[BPY]^+[NO_3]^-$-TS < $[BPY]^+[NO_3]^-$-BT < $[BPY]^+[NO_3]^-$-DBT. The results suggested that the selective extraction followed the order of DBT > BT > TS > NAP. The sequence of interaction energies between $[BPY]^+[NO_3]^-$ and TS, BT, DBT, NAP is in agreement with the selective extraction trend of experimental results.[19] The interaction energies are different with or without DFT-D method, but the changing trend is similar.

NBO Analysis. NBO analyses for TS, BT, DBT, NAP, $[BPY]^+[NO_3]^-$, $[BPY]^+[NO_3]^-$-TS, $[BPY]^+[NO_3]^-$-BT, $[BPY]^+[NO_3]^-$-DBT and $[BPY]^+[NO_3]^-$-NAP were carried out to obtain the charge distribution and intrinsic property of the interactions between $[BPY]^+[NO_3]^-$ and TS, BT, DBT, NAP. From NBO atomic charges, most of the positive charge is focused on the peripheral hydrogen atoms of pyridinium ring and butyl hydrogen atoms in $[BPY]^+$ cation. While $[NO_3]^-$ anion preferentially approaches the positively charged groups, indicating that the electrostatic interaction between $[BPY]^+$ cation and $[NO_3]^-$ anion is dominative for the formation of ion pair. The sums of charges of $[NO_3]^-$ in $[BPY]^+[NO_3]^-$, $[BPY]^+[NO_3]^-$-TS, $[BPY]^+[NO_3]^-$-BT, $[BPY]^+[NO_3]^-$-DBT and $[BPY]^+[NO_3]^-$-NAP are –0.88946, –0.91211, –0.92066, –0.90247, –0.91314, suggesting that the negative charges migrate from $[NO_3]^-$ to other parts. It is clear that the TS, BT, DBT or NAP adsorptions on $[BPY]^+[NO_3]^-$ have influences on the distribution of the charges in $[BPY]^+[NO_3]^-$ and TS, BT, DBT or NAP. Compared with the NBO charges, the positive charge of H and negative charge of O increase when they are involved in H···O interactions. The shorter contact of H···O, the more increase of positive charges of hydrogen atoms and negative charges of oxygen atoms. The interactions between O of $[NO_3]^-$ and TS, BT, DBT, NAP increase the negative charges of O, resulting in the less negative charge migration of $[NO_3]^-$ in $[BPY]^+[NO_3]^-$-TS (–0.91211), $[BPY]^+[NO_3]^-$-BT (–0.92066), $[BPY]^+[NO_3]^-$-DBT (–0.90247) and $[BPY]^+[NO_3]^-$-NAP (–0.91314) in contrast with that of $[BPY]^+[NO_3]^-$ (–0.88946).

Nowadays it seems quite well accepted that hydrogen bonding influences the structures of ionic liquids. NBO method can provide information about the interactions in both filled and virtual orbital spaces that facilitates analysis of the intermolecular interactions. A second-order perturbation theory analysis of the Fock matrix was carried out to evaluate the donor-acceptor interaction in the NBO basis. In this analysis, a stabilization energy $E(2)$ related to the delocalization trend of electrons from donor to acceptor orbitals was calculated via perturbation theory. If the stabilization energy $E(2)$ between a donor bonding orbital and an acceptor orbital is large, then there is a strong interaction between them. Table 1 lists the selected donor-acceptor interactions

Table 1. Some donor-acceptor interactions in $[BPY]^+[NO_3]^-$, $[BPY]^+[NO_3]^-$-TS, $[BPY]^+[NO_3]^-$-BT, $[BPY]^+[NO_3]^-$-DBT, $[BPY]^+[NO_3]^-$-NAP and their second order perturbation stabilization energies, $E(2)$ (kcal/mol)

Donor	Acceptor	$E(2)$ (kcal/mol)	Donor	Acceptor	$E(2)$ (kcal/mol)
		$[BPY]^+[NO_3]^-$			
LP(O1)	σ*(C2-H2)	1.35	LP(O1)	σ*(C7-H71)	9.57
LP(O1)	σ*(C2-C3)	0.08	LP(O1)	π*(C2-N1)	0.67
LP(O2)	σ*(C2-H2)	18.33	LP(O2)	σ*(C8-H81)	1.15
LP(O2)	σ*(C2-C3)	0.07	LP(O2)	π*(C2-N1)	0.09
		$[BPY]^+[NO_3]^-$-TS			
σ(C8-H81)	σ*(N-O3)	0.06	π(C4-C3)	π*(C4'-C5')	0.07
π*(C4-C3)	π*(C4'-C5')	0.05	π*(C2-N1)	π*(C2'-C3')	0.09
LP(O1)	σ*(C2-H2)	14.75	LP(O1)	σ*(C7-H72)	2.88
LP(O1)	σ*(C2-C3)	0.07	LP(O3)	σ*(C7-H72)	0.58
LP(O3)	σ*(C8-H82)	0.22	LP(O3)	σ*(C8-H81)	0.71
LP(O3)	π*(C2-N1)	0.45	LP(O3)	σ*(C2-H2)	0.20
LP(O3)	σ*(C7-H71)	0.17	LP(O3)	σ*(C9-H92)	0.23
σ*(N-O2)	σ*(C2-H2)	0.26	σ*(N-O2)	σ*(C7-H72)	0.13
LP(O3)	σ*(C2'-H2')	0.08	LP(O3)	σ*(S-C5')	0.30
LP(O2)	σ*(C2'-H2')	1.12	π(C2'-C3')	π*(C4-C3)	0.19
π(C2'-C3')	σ*(C3-H3)	0.20	LP(S)	σ*(C8-H81)	0.21
LP(S)	π*(C4-C3)	0.20	LP(S)	π*(C2-N1)	0.90
π*(C2'-C3')	σ*(C3-H3)	0.06			
		$[BPY]^+[NO_3]^-$-BT			
π*(C4-C3)	π*(C7a-C3a)	1.26	π*(C4-C3)	π*(C3'-C2')	0.24
π*(C5-C6)	π*(C7'-C7a)	0.12	σ(C2-H2)	σ*(O3-N)	0.07
π(C7a-C3a)	π*(C4-C3)	0.17	π(C7'-C7a)	π*(C5-C6)	0.10
π(C3'-C2')	π*(C4-C3)	0.15	π(C3'-C2')	σ*(C3-H3)	0.09
π(C4'-C5')	σ*(C8-H81)	0.12	LP(S)	π*(C4-C3)	0.22
LP(S)	σ*(C4-H4)	0.52	LP(O3)	σ*(C8-H81)	0.98
LP(O2)	σ*(C2-N1)	0.26	LP(O2)	σ*(C2-H2)	1.07
LP(O2)	π*(C2-N1)	0.99	LP(O2)	π*(C4-C3)	0.06
LP(O1)	σ*(C2-H2)	8.78	LP(O1)	σ*(C7-H71)	1.63
LP(O1)	σ*(C9-H91)	0.11	LP(O1)	σ*(C3-C2)	0.09
LP(O1)	σ*(C7-H72)	0.20	LP(O1)	σ*(C8-H82)	0.07
LP(O3)	σ*(C4'-H4')	2.36	LP(O2)	π*(C3'-C2')	0.20
LP(O2)	σ*(C3'-H3')	0.98			
		$[BPY]^+[NO_3]^-$-DBT			
σ(C8-H81)	σ(N-O3)	0.10	π*(C2-N1)	π*(O2-N)	0.81
π(C4-C3)	π*(C13'-C10')	0.11	π(C4-C3)	π*(C11'-C12')	0.14
π*(C4-C3)	π*(C13'-C10')	0.44	π*(C4-C3)	π*(C11'-C12')	0.70
π*(C4-C3)	π*(C1'-C2')	0.09	σ(N-O2)	σ*(C2-H2)	0.08
σ(N-O1)	σ*(C2-H2)	0.16	σ(N-O3)	σ*(C2-H2)	0.06
LP(O1)	σ*(C2-H2)	14.63	LP(O1)	σ*(C7-H71)	1.70
LP(O1)	σ*(C3-C2)	0.07	LP(O3)	π*(C2-N1)	2.81
LP(O3)	σ*(C8-H81)	2.88	LP(O3)	σ*(C2-H2)	0.14
LP(O3)	σ*(C7-H72)	0.15	σ*(N-O2)	σ*(C2-H2)	0.26
LP(O2)	σ*(C1'-H1')	0.22	LP(O3)	σ*(C9'-H9')	0.63
LP(O3)	σ*(C1'-H1')	2.54	LP(O3)	π*(C1'-C2')	0.20
π(C13'-C10')	π*(C4-C3)	0.69	π(C6'-C7')	π*(C5-C6)	0.26
π(C11'-C12')	π*(C4-C3)	0.11	π (C1'-C2')	π*(C4-C3)	0.06
LP(S5)	σ*(C4-H4)	0.49			
		$[BPY]^+[NO_3]^-$-NAP			
π(C4-C3)	π*(C9'-H10')	0.09	π*(C4-C3)	π*(C6'-C5')	0.10
LP(O1)	σ*(C2-N1)	0.06	LP(O1)	σ*(C2-H2)	14.19
LP(O1)	π*(C2-N1)	0.44	LP(O3)	σ*(C7-H71)	6.07
LP(O3)	σ*(C9-H91)	1.67	LP(O3)	σ*(C2-H2)	0.06
LP(O3)	σ*(C7-H72)	0.07	LP(O2)	σ*(C8-H81)	0.34
LP(O1)	π*(C1'-C2')	0.43	LP(O1)	σ*(C2'-H2')	0.12
LP(O2)	σ*(C2'-H2')	2.11	π(C7'-C8')	π*(C5-C6)	0.13
π(C6'-C5')	π*(C4-C3)	0.34	π(C6'-C5')	σ*(C4-H4)	0.12
π(C1'-C2')	π*(C2-N1)	0.51	π(C1'-C2')	σ*(C8-H81)	0.26
π(C4'-C3')	π*(C4-C3)	0.52	π(C4'-C3')	σ*(C3-H3)	0.22

Table 2. The topological properties of electron density (ρ), Laplacian of density ($\nabla^2\rho$), eigenvalues of the Hessian matrix (λ_1, λ_2, λ_3) of $[BPY]^+[NO_3]^-$, $[BPY]^+[NO_3]^-$-TS, $[BPY]^+[NO_3]^-$-BT, $[BPY]^+[NO_3]^-$-DBT and $[BPY]^+[NO_3]^-$-NAP (atomic units)

X···Y	cp type	D/Å	ρ	$\nabla^2\rho$	λ_1	λ_2	λ_3
				$[BPY]^+[NO_3]^-$			
O1···H71	(3, −1)	2.082	0.02203	0.05974	-0.02707	-0.02489	0.11169
O2···H2	(3, −1)	1.911	0.03107	0.08053	-0.04272	-0.04039	0.16364
O2···H81	(3, −1)	2.608	0.00802	0.02710	-0.00729	-0.00635	0.04074
PY ring	(3, +1)	···	0.02137	0.17005	-0.01779	0.08793	0.09991
				$[BPY]^+[NO_3]^-$-TS			
O1···H2	(3, −1)	1.929	0.02927	0.07842	-0.03924	-0.03656	0.15423
O1···H72	(3, −1)	2.447	0.01116	0.03415	-0.01092	-0.00941	0.05449
O2···H2'	(3, −1)	2.380	0.01092	0.03483	-0.01097	-0.01020	0.05601
O3···H72	(3, −1)	2.639	0.00829	0.03093	-0.00670	-0.00385	0.04149
O3···H81	(3, −1)	2.528	0.00887	0.03284	-0.00769	-0.00626	0.04679
O3···S	(3, −1)	3.371	0.00598	0.02189	-0.00362	-0.00251	0.02804
S···H81	(3, −1)	3.400	0.00262	0.00835	-0.00146	-0.00131	0.01112
S···C2	(3, −1)	3.576	0.00603	0.01683	-0.00315	-0.00143	0.02142
H3···C3'	(3, −1)	3.030	0.00466	0.01459	-0.00241	-0.00129	0.01829
PY ring	(3, +1)	···	0.02143	0.17062	-0.01788	0.08835	0.10015
TS ring	(3, +1)	···	0.03795	0.26562	-0.03610	0.14269	0.15902
				$[BPY]^+[NO_3]^-$-BT			
O2···H3'	(3, −1)	2.548	0.00799	0.02918	-0.00758	-0.00616	0.04292
O1···H2	(3, −1)	2.054	0.02324	0.06546	-0.02796	-0.02621	0.11963
O1···H71	(3, −1)	2.386	0.01196	0.04129	-0.01078	-0.01022	0.06231
O1···H81	(3, −1)	2.820	0.00609	0.02352	-0.00412	-0.00069	0.02834
O3···H81	(3, −1)	2.658	0.00668	0.02364	-0.00568	-0.00482	0.03414
O3···H4'	(3, −1)	2.462	0.00973	0.03061	-0.00987	-0.00922	0.04971
C3'···C3	(3, −1)	3.507	0.00459	0.01325	-0.00232	-0.00058	0.01616
H4···S	(3, −1)	3.081	0.00592	0.01912	-0.00427	-0.00297	0.02637
C7a··C4	(3, −1)	3.458	0.00496	0.01394	-0.00207	-0.00119	0.01721
PY ring	(3, +1)	···	0.02142	0.17065	-0.01785	0.08834	0.10016
TS ring	(3, +1)	···	0.03611	0.24937	-0.03416	0.12932	0.15421
BZ ring	(3, +1)	···	0.02026	0.15685	-0.01591	0.08171	0.09104
				$[BPY]^+[NO_3]^-$-DBT			
O1···H2	(3, −1)	1.940	0.02896	0.07815	-0.03847	-0.03627	0.15290
O1···H71	(3, −1)	2.563	0.00896	0.02948	-0.00856	-0.00606	0.04410
O3···H2	(3, −1)	2.424	0.01343	0.05287	-0.01209	-0.00443	0.06940
O3···H81	(3, −1)	2.312	0.01324	0.04365	-0.01368	-0.01241	0.06975
O3···H1'	(3, −1)	2.368	0.01233	0.03890	-0.01289	-0.01148	0.06328
O3···H9'	(3, −1)	2.616	0.00622	0.02364	-0.00514	-0.00489	0.03368
C5···C8'	(3, −1)	3.786	0.00356	0.00891	-0.00100	-0.00066	0.01058
C10'···C4	(3, −1)	3.343	0.00634	0.01781	-0.00334	-0.00063	0.02179
C11'···C3	(3, −1)	3.389	0.00556	0.01633	-0.00282	-0.00073	0.01989
S5···H4	(3, −1)	3.119	0.00526	0.01749	-0.00367	-0.00183	0.02299
PY ring	(3, +1)	···	0.02143	0.17053	-0.01785	0.08863	0.09975
TS ring	(3, +1)	···	0.03433	0.23409	-0.03242	0.11862	0.14789
BZ ring1	(3, +1)	···	0.02045	0.15778	-0.01603	0.08321	0.09061
BZ ring2	(3, +1)	···	0.02051	0.15879	-0.01609	0.08365	0.09122
				$[BPY]^+[NO_3]^-$-NAP			
O1···H2	(3, −1)	1.946	0.02778	0.07584	-0.03721	-0.03397	0.14703
O1···H2'	(3, −1)	2.784	0.00659	0.02472	-0.00505	-0.00228	0.03206
O3···H71	(3, −1)	2.169	0.01809	0.05334	-0.02072	-0.01892	0.09300
O3···H91	(3, −1)	2.523	0.00938	0.03068	-0.00927	-0.00800	0.04796
O2···H2'	(3, −1)	2.491	0.00942	0.03016	-0.00922	-0.00894	0.04833
O2···H81	(3, −1)	2.825	0.00502	0.01916	-0.00377	-0.00259	0.02553
C8'···C5	(3, −1)	3.810	0.00318	0.00839	-0.00110	-0.00038	0.00988
C10'···C3	(3, −1)	3.407	0.00589	0.01642	-0.00251	-0.00068	0.01962
PY ring	(3, +1)	···	0.02141	0.17034	-0.01783	0.08814	0.10003
BZ ring1	(3, +1)	···	0.01997	0.15452	-0.01577	0.08416	0.08613
BZ ring2	(3, +1)	···	0.01991	0.15417	-0.01569	0.08351	0.08634

in $[BPY]^+[NO_3]^-$, $[BPY]^+[NO_3]^-$-TS, $[BPY]^+[NO_3]^-$-BT, $[BPY]^+[NO_3]^-$-DBT and $[BPY]^+[NO_3]^-$-NAP and their second order perturbation stabilization energies. As indicated in Table 1, the C2-H2 involved hydrogen bonds are strongest, in terms of the large $E(2)$ of 18.33 kcal/mol (LP(O2) → σ*(C2-H2)) in $[BPY]^+[NO_3]^-$, 14.75 kcal/mol (LP(O1) → σ*(C2-H2)) in $[BPY]^+[NO_3]^-$-TS, 8.78 kcal/mol (LP(O1) → σ*(C2-H2)) in $[BPY]^+[NO_3]^-$-BT, 14.63 kcal/mol (LP(O1) → σ*(C2-H2)) in $[BPY]^+[NO_3]^-$-DBT, and 14.19 kcal/mol (LP(O1) → σ*(C2-H2)) in $[BPY]^+[NO_3]^-$-NAP, in agreement with their short O···H contacts.

Table 1 shows that hydrogen bonding (LP(O) → σ*(C-H)), π···σ and π···π interactions occur between $[BPY]^+[NO_3]^-$ and TS, $[BPY]^+[NO_3]^-$ and NAP, hydrogen bonding (LP(O) → σ*(C-H)), LP(O)···σ, LP(O)···π, π···σ and π···π interactions exist between $[BPY]^+[NO_3]^-$ and BT, $[BPY]^+[NO_3]^-$ and DBT. The π···π interactions between $[BPY]^+[NO_3]^-$ and DBT are the strongest among π···π interactions between $[BPY]^+[NO_3]^-$ and TS, BT, DBT, NAP. It is noted that the charges of sulfur of TS, BT, and DBT are +0.45527, +0.43055 and +0.42110, while the sulfur-involved interactions of LP(O3) → σ*(S-C5') (0.30 kcal/mol), LP(S) → σ*(C8-H81) (0.21 kcal/mol), LP(S) → π*(C2-N1) (0.90 kcal/mol), LP(S) → π*(C4-C3) (0.20 kcal/mol) in $[BPY]^+[NO_3]^-$-TS, LP(S) →

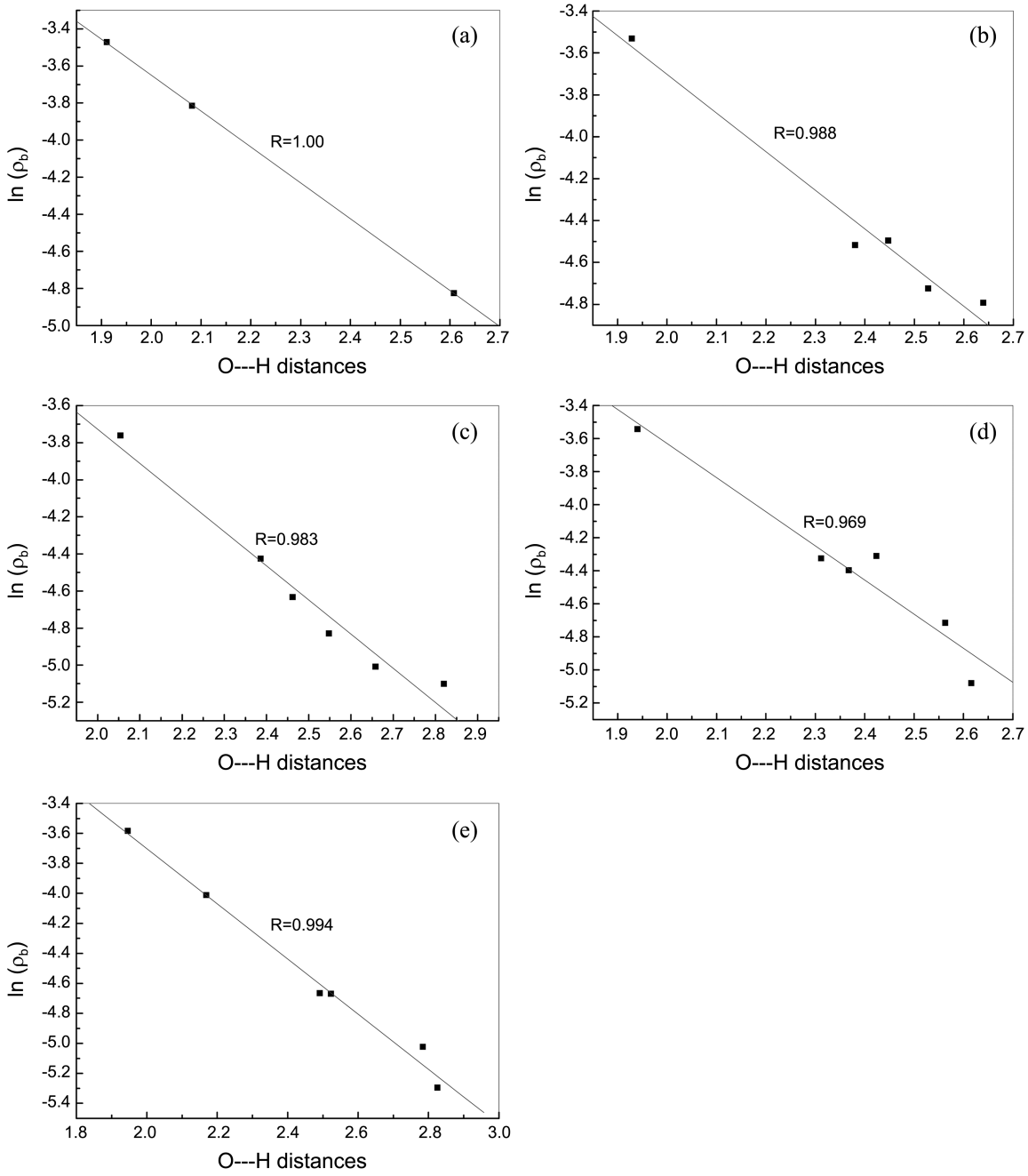

Figure 4. Plots of the regressions between the O···H distances and their corresponding $\ln(\rho_b)$ of (a) $[BPY]^+[NO_3]^-$, (b) $[BPY]^+[NO_3]^-$-TS, (c) $[BPY]^+[NO_3]^-$-BT, (d) $[BPY]^+[NO_3]^-$-DBT and (e) $[BPY]^+[NO_3]^-$-NAP.

π*(C4-C3) (0.22 kcal/mol), LP(S) → σ*(C4-H4) (0.52 kcal/mol) in $[BPY]^+[NO_3]^-$-BT, LP(S5) → σ*(C4-H4) (0.49 kcal/mol) in $[BPY]^+[NO_3]^-$-DBT suggest that the strength of sulfur-involved interactions is TS > BT > DBT, which may be ascribed to the steric hindrance.

AIM Analyses. The bond properties between each pair of atoms were systematically analyzed using quantum theory of atoms in molecules (AIM),[38] which is based on the topological analysis of electron density (ρ) and its Laplacian ($\nabla^2\rho$) at the bond critical points (BCPs). Covalent bonding is characterized by $\nabla^2\rho < 0$, while closed-shell bonding interaction is characterized by a depletion of density in the region of contact of the two atoms and $\nabla^2\rho > 0$. Electron density (ρ) is used to describe the strength of a bond, a stronger bond associated with a larger ρ value. The bond characteristics for the $[BPY]^+[NO_3]^-$, $[BPY]^+[NO_3]^-$-TS, $[BPY]^+[NO_3]^-$-BT, $[BPY]^+[NO_3]^-$-DBT and $[BPY]^+[NO_3]^-$-NAP were provided in Table 2 based on AIM analysis. The first evidence of interactions according to the AIM approach is the existence of a bond path between two atoms and the existence of a bond critical point (BCP).[39,40] From the values of electron density listed in Table 2, it can be concluded that the interactions between $[BPY]^+[NO_3]^-$ and TS, BT, DBT, NAP are all closed-shell systems in terms of positive values of $\nabla^2\rho$. A second AIM criterion to define hydrogen bond is that electron density (ρ) and the Laplacian of electron density ($\nabla^2\rho$) at BCP must be within 0.002-0.035 au and 0.024-0.139 au ranges, respectively.[39,40] These values are within the commonly accepted values, indicating the occurrence of hydrogen bonding interactions of these systems. The topological properties of the bond critical points of O3···S (ρ = 0.00598 au, $\nabla^2\rho$ = 0.02189 au), S···H81 (ρ = 0.00262 au, $\nabla^2\rho$ = 0.00835 au), S···C2 (ρ = 0.00603 au, $\nabla^2\rho$ = 0.01683 au), H3···C3' (ρ = 0.00466 au, $\nabla^2\rho$ = 0.01459 au) in $[BPY]^+[NO_3]^-$-TS, C3'···C3 (ρ = 0.00459 au, $\nabla^2\rho$ = 0.01325 au), H4···S (ρ = 0.00592 au, $\nabla^2\rho$ = 0.01912 au), C7a··C4 (ρ = 0.00496 au, $\nabla^2\rho$ = 0.01394 au) in $[BPY]^+[NO_3]^-$-BT, C5···C8' (ρ = 0.00356 au, $\nabla^2\rho$ = 0.00891 au), C10'···C4 (ρ = 0.00634 au, $\nabla^2\rho$ = 0.01781 au), C11'···C3 (ρ = 0.00556 au, $\nabla^2\rho$ = 0.01633 au), S5···H4 (ρ = 0.00526 au, $\nabla^2\rho$ = 0.01749 au) in $[BPY]^+[NO_3]^-$-DBT, C8'···C5 (ρ = 0.00318 au, $\nabla^2\rho$ = 0.00839 au), C10'···C3 (r = 0.00589 au, $\nabla^2\rho$ = 0.01642 au) in $[BPY]^+[NO_3]^-$-NAP, demonstrate that π···π interactions occur between $[BPY]^+[NO_3]^-$ and TS, BT, DBT, NAP, but π···π interactions between $[BPY]^+[NO_3]^-$ and DBT are the strongest. It can also show that sulfur atoms involved interactions between $[BPY]^+[NO_3]^-$ and TS, BT, DBT are TS > BT > DBT, in agreement with the NBO analyses.

Sainz-Diaz *et al*. indicated that the dipole moment value increases following the sequence: TS < BT < DBT. The energy gap between highest occupied molecular orbital and lowest unoccupied molecular orbital (E_{HOMO}–E_{LUMO}) decreases following the sequence: TS < BT < DBT. This can be explained by the increase of the aromatic electron delocalization and hence the decrease of the energy difference between electronic levels increasing the absorption capacity.[41] Su *et al.* proved that molecules with highly polarizable π-electron density preferably insert into the molecular structure of the ionic liquids.[13] Zhang *et al.* also stated that the sulfur compounds with a higher density of aromatic π-electron are favorably absorbed by ionic liquids.[42,43] The relatively large differences in the partition coefficients of the individual sulfur compounds may be due to the difference of aromatic π-electron density of sulfur compounds. These results suggested that the extractive performance becomes better with the increase of the aromatic π-electron density.[22] According to our NBO and AIM analyses, the different interactions between $[BPY]^+[NO_3]^-$ and TS, BT, DBT may be ascribed to different strength of π-π interactions. While π-π interactions may be attributed to the difference of aromatic π-electron density of TS, BT, and DBT. The polar aromatic TS may have stronger interactions with the charged ion pair of ionic liquid than non-polar aromatic NAP.

As seen in Table 2, the values of electron density for hydrogen bonding interactions in all configurations decrease with the increase of interacting distances. This decrease in electron density in BCPs can be ascribed to decrease of interaction energy. For hydrogen bonds, there is a correlation between the interaction distances and topological parameters at the BCPs.[44,45] Here, the existence of such a correlation has been checked for configurations $[BPY]^+[NO_3]^-$, $[BPY]^+[NO_3]^-$-TS, $[BPY]^+[NO_3]^-$-BT, $[BPY]^+[NO_3]^-$-DBT and $[BPY]^+[NO_3]^-$-NAP. Figure 4 presents the linear correlation between O···H distances and their corresponding $\ln(\rho_b)$ in $[BPY]^+[NO_3]^-$, $[BPY]^+[NO_3]^-$-TS, $[BPY]^+[NO_3]^-$-BT, $[BPY]^+[NO_3]^-$-DBT and $[BPY]^+[NO_3]^-$-NAP, confirming the dependence between hydrogen bonding strength and their distances. So the topological properties are useful descriptors for the strength of hydrogen bonds.

Conclusion

In order to deepen the understanding of interactions between *N*-butylpyridinium nitrate ($[BPY]^+[NO_3]^-$) ionic liquid and thiophene (TS), benzothiophene (BT), dibenzothiophene (DBT), naphthalene (NAP), the structures of $[BPY]^+[NO_3]^-$, $[BPY]^+[NO_3]^-$-TS, $[BPY]^+[NO_3]^-$-BT, $[BPY]^+[NO_3]^-$-DBT and $[BPY]^+[NO_3]^-$-NAP were optimized using density functional theory, and their most stable geometries were discussed in terms of NBO and AIM analyses. The results show that the multiple intermolecular hydrogen bonds play an important role in stabilizing $[BPY]^+[NO_3]^-$ pair. The predominant interaction of C2-H2···O was not changed by adsorption of TS, BT, DBT, NAP. The NBO and AIM analyses proved that the π···π and hydrogen bonding interactions occur between $[BPY]^+[NO_3]^-$ and TS, BT, DBT, NAP. But the π···π and hydrogen bonding interactions between $[BPY]^+[NO_3]^-$ and NAP are weak. DBT is prior to adsorption on $[BPY]^+[NO_3]^-$ ionic liquid. The different interactions between $[BPY]^+[NO_3]^-$ and TS, BT, DBT may be assigned to different strength of π-π interactions.

Acknowledgments. The authors gratefully acknowledge financial support from the Natural Science Foundation of

China (21176259), awarded foundation for excellent young and middle-aged scientist of Shandong Province, China (BS2010NJ024) and the Natural Science Foundation of Shandong Province (ZR2011BQ004, ZR2011BQ020), China. And the publication cost of this paper was supported by the Korean Chemical Society.

References

1. Stanislaus, A.; Marafi, A.; Rana, M. S. *Catal. Today* **2010**, *153*, 1.
2. Kulkarni, P. S.; Afonso, C. A. M. *Green Chem*. **2010**, *12*, 1139.
3. Bosmann, A.; Datsevich, L.; Jess, A.; Lauter, A.; Schmitz, C.; Wasseerscheid, P. *Chem. Commun.* **2001**, 2494.
4. Lo, W.; Yang, H.; Wei, G. *Green Chem*. **2003**, *5*, 639.
5. Anantharaj, R.; Banerjee, T. *Int. J. Chem. Eng*. **2011**, *2011*, 1.
6. Potdar, S.; Anantharaj, R.; Banerjee, T. *J. Chem. Eng. Data* **2012**, *57*, 1026.
7. Kumar, A. A. P.; Banerjee, T. *Fluid Phase Equilib*. **2009**, *278*, 1.
8. Anantharaj, R.; Banerjee, T. *Fluid Phase Equilib*. **2011**, *312*, 20.
9. Santiago, R. S.; Santos, G. R.; Aznar, M. *Fluid Phase Equilib*. **2009**, *278*, 54.
10. Hanke, C. G.; Johansson, A.; Harper, J. B.; Lynden-Bell, R. M. *Chem. Phys. Lett*. **2003**, *374*, 85.
11. Kedra-Krolik, K.; Fabrice, M.; Jaubert, J. *Ind. Eng. Chem. Res*. **2011**, *50*, 2296.
12. Anantharaj, R.; Banerjee, T. *AIChE J*. **2011**, *57*, 749.
13. Su, B.; Zhang, S.; Zhang, C. *J. Phys. Chem. B* **2004**, *108*, 19510.
14. Zhou, J.; Mao, J.; Zhang, S. *Fuel Process. Technol*. **2008**, *89*, 1456.
15. Martinez-Magadan, J.; Oviedo-Roa, R.; Garcia, P.; Martinez-Palou, R. *Fuel Process. Technol*. **2012**, *97*, 24.
16. Liu, X.; Zhou, G.; Zhang, X.; Zhang, S. *AIChE J*. **2010**, *56*, 2983.
17. Gui, J.; Liu, D.; Sun, Z.; Liu, D.; Min, D.; Song, B.; Peng, X. *J. Mol. Catal. A: Chem*. **2010**, *331*, 64.
18. Nie, Y.; Yuan, X. *J. Theor. Comput. Chem*. **2011**, *10*, 31.
19. Wang, J.; Zhao, D.; Zhou, E.; Dong, Z. *J. Fuel Chem. Technol.* **2007**, *35*, 293.
20. Gao, H.; Luo, M.; Xing, J.; Wu, Y.; Li, Y.; Li, W.; Liu, Q.; Liu, H. *Ind. Eng. Chem. Res.* **2008**, *47*, 8384.
21. Zhao, D.; Wang, Y.; Duan, E. *Molecules* **2009**, *14*, 4351.
22. Gao, H.; Li, Y.; Wu, Y.; Luo, M.; Li, Q.; Xing, J.; Liu, H. *Energy Fuels* **2009**, *23*, 2690.
23. Zhao, D.; Wang, Y.; Duan, E.; Zhang, J. *Chem. J. Chin. Univ.* **2010**, *31*, 488.
24. Delley, B. *J. Chem. Phys.* **1990**, *92*, 508.
25. Delley, B. *J. Chem. Phys*. **2000**, *113*, 7756.
26. Perdew, J. P.; Wang, Y. *Phys. Rev. B* **1992**, *45*, 13244.
27. Castellano, O.; Gimon, R.; Soscun, H. *Energy Fuels* **2011**, *25*, 2526.
28. Reed, A. E.; Curtiss, L. A.; Weinhold, F. *Chem. Rev.* **1988**, *88*, 899.
29. Singh, R. N.; Kumar, A.; Tiwari, R. K.; Rawat, P.; Gupta, V. P. *J. Mol. Struct*. **2013**, *1035*, 427.
30. Lobayan, R. M.; Jubert, A. H.; Vitale, M. G.; Pomilio, A. B. *J. Mol. Model* **2009**, *15*, 537.
31. Biegler-König, F.; Schönbohm, J. *J. Comput. Chem.* **2002**, *23*, 1489.
32. Biegler-König, F.; Schönbohm, J.; Bayles, D. *J. Comput. Chem.* **2001**, *22*, 545.
33. Inada, Y.; Orita, H. *J. Comput. Chem.* **2008**, *29*, 225.
34. Bondi, A. *J. Phys. Chem.* **1964**, *68*, 441.
35. Sinnokrot, M. O.; Valeev, E. F.; Sherrill, C. D. *J. Am. Chem. Soc.* **2002**, *124*, 10887.
36. Hunter, C. A.; Sanders, J. K. M. *J. Am. Chem. Soc.* **1990**, *112*, 5525.
37. Rashkin, M. J.; Waters, M. L. *J. Am. Chem. Soc.* **2002**, *124*, 1860.
38. Bader, R. W. F. *Chem. Rev.* **1991**, *91*, 893.
39. Koch, U.; Popelier, P. L. A. *J. Phys. Chem*. **1995**, *99*, 9747.
40. Popelier, P. L. A. *J. Phys. Chem. A* **1998**, *102*, 1873.
41. Sainz-Diaz, C. I.; Francisco-Marquez, M.; Vivier-Bunge, A. *Theor. Chem. Acc*. **2010**, *125*, 83.
42. Zhang, S.; Zhang, Z. C. *Green Chem.* **2002**, *4*, 376.
43. Zhang, S.; Zhang, Q.; Zhang, Z. C. *Ind. Eng. Chem. Res.* **2004**, *43*, 614.
44. Espinosa, E.; Souhassou, M.; Lachekar, H.; Lecomte, C. *Acta Cryst*. **1999**, *B55*, 563.
45. Netzel, J.; van Smaalen, S. *Act Cryst*. **2009**, *B65*, 624.